

# Estimation of the Cardiac Field in the Esophagus Using a Multipolar Esophageal Catheter

Reto Andreas Wildhaber <sup>1b</sup>, Dominik Bruegger, Nour Zalmi, Hampus Malmberg, Josef Goette, Marcel Jacomet, Hildegard Tanner, Andreas Haerberlin, and Hans-Andrea Loeliger, *Fellow, IEEE*

**Abstract**—The rapid progress of invasive therapeutic options for cardiac arrhythmias increases the need for accurate diagnostics. The surface electrocardiogram (ECG) is still the standard of noninvasive diagnostics but lacks atrial signal resolution. By contrast, esophageal electrocardiography (EECG) yields atrial signals of high amplitude and with a high signal-to-noise ratio. Esophageal electrocardiography has become fast and safe, but the mechanical constraints of esophageal measuring catheters and the “random” motion of the catheter inside the subject’s esophagus limit the spatial resolution of EECG signals. In this paper, we propose a method to estimate the electrical field projected onto the esophagus with an increased spatial resolution, using commonly available esophageal catheters. In a first step, we estimate the time-varying catheter position, and in a second step, we estimate the projected electrical field with enhanced spatial resolution. The proposed algorithm comprises several consecutive optimization steps, where each intermediate step produces not just a single point estimate, but a cost function over multiple solutions, which reduces the information loss at each processing step. We conclude with examples from a clinical trial, where the fields of cardiac arrhythmias are presented as two-dimensional contour plots.

**Index Terms**—Algorithm, arrhythmia diagnostics, cardiac arrhythmias, esophageal electrocardiography, medical device, multi-channel signal processing, signal reconstruction.

## I. INTRODUCTION

FOR more than half a century, the standard 3-lead and 12-lead electrocardiogram (ECG) have been the most important diagnostic tools in cardiology. Despite its popularity,

Manuscript received November 16, 2017; accepted February 15, 2018. This work was supported by the Swiss National Science Foundation under Grant CR23I2\_166030. This paper was recommended by Associate Editor M. Milanova. (Corresponding author: Reto Andreas Wildhaber.)

R. A. Wildhaber is with the Department of Information Technology and Electrical Engineering, ETH Zurich, Zurich 8092, Switzerland, and also with the Institute for Human Centered Engineering, Bern University of Applied Sciences, Biel 2500, Switzerland (e-mail: reto.wildhaber@bfh.ch).

D. Bruegger, J. Goette, and M. Jacomet are with the Institute for Human Centered Engineering, Bern University of Applied Sciences, Biel 2500, Switzerland (e-mail: dominik.bruegger@bfh.ch; josef.goette@bfh.ch; marcel.jacomet@bfh.ch).

N. Zalmi, H. Malmberg, and H.-A. Loeliger are with the, Department of Information Technology and Electrical Engineering, ETH Zurich, Zurich 8092, Switzerland (e-mail: zalmi@isi.ee.ethz.ch; malmberg@isi.ee.ethz.ch; loeliger@isi.ee.ethz.ch).

H. Tanner and A. Haerberlin are with the Department of Cardiology, Inselspital, Bern University Hospital, Bern 3010, Switzerland, and also with the University of Bern, Bern 3012, Switzerland (e-mail: Hildegard.Tanner@insel.ch; andreas.haerberlin@insel.ch).

Color versions of one or more of the figures in this paper are available online at <http://ieeexplore.ieee.org>.

Digital Object Identifier 10.1109/TBCAS.2018.2817027

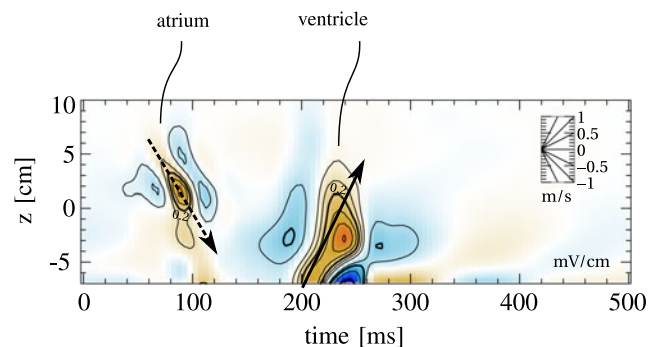


Fig. 1. Example of the estimated (projected) cardiac electric field, observed along the esophagus and depicted as a two-dimensional (2D) contour plot; named an esophageal isopotential map (IPM). An IPM shows the position along the esophagus on the vertical axis ( $z$ ) and the time progress on the horizontal axis. The 2D plot is additionally shaded in colors according to the electric field’s strength (positive values in orange/red, negative values in blue). The atrial signal in this example shows a propagation from top to bottom (i.e., cranio-caudal, dashed arrow), while the propagation in the ventricle runs from bottom to top (i.e., caudo-cranial, solid arrow).

common surface ECGs have some limitations, in particular for questions in rhythmology, due to the limited atrial (P wave) resolution. The rapid progress of invasive therapeutic options for cardiac arrhythmias increases the need for more accurate diagnostics. Esophageal electrocardiography (EECG) is an alternative low-risk electrocardiogram recording method. Due to the anatomical proximity of the esophagus to the heart atria, EECG signals offer high atrial resolution [1], [2].

Experiments with esophageal electrocardiography began already around 1906 [3], but EECG has so far remained a niche technology. There might be various reasons for this development: probably the surface ECG method was superior for the emerging questions at that time and with growing experience accumulated over decades, it was hard for any alternatives to establish themselves. Finally, patient tolerance issues and the increased technical complexity may have additionally prevented the EECG procedure to spread very far.

Nowadays, materials and techniques have highly improved; thin and soft catheter tubes are inserted through the nose, an already well established route from the application of feeding tubes, and reach any location in the esophagus. If needed, local surface anesthesia is sufficient to avoid discomfort and pain during this fast and safe procedure.

While the equipment hurdles are decently solved, esophageal electrodes preserved their own characteristics: while surface

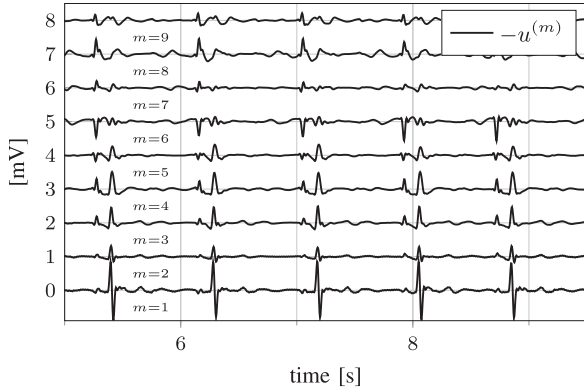


Fig. 2. Multi-channel esophageal ECG signal. Most proximal channel ( $m = 9$ ) is shown at top. In accordance to the convention used for surface ECG signals, the plot displays the negative voltage  $-u$  instead of  $u$ . To improve readability, an individual offset of 0 to 8 mV was added to each channel.

electrodes stick to a particular skin location, esophageal electrodes drift inside the esophagus and their location vary with the peristalses and the patient's body or breathing motions. In other words, esophageal electrodes, as they are usually applied, do not stick to a single location, which requires proper tracking of the current electrode locations for any application depending on sufficient spatial resolution.

In this paper, we propose a method to estimate the electric field projected onto the esophagus with a high spatial resolution. For that we use EECG signals recorded using common esophageal catheters and present the resulting field estimate as a two-dimensional (2D) contour plot. With these contour plots we intend to complement the 12-lead ECG records and to address particular questions in rhythmology.

To estimate the field, we first give a method to track the varying catheter position relative to the heart using the esophageal signals only. In a second step we estimate the projected electric field with a high spatial resolution. Esophageal catheters usually have a wide electrode spacing and a limited number of electrodes (e.g. 4 to 10 electrodes). But wide electrode spacing leads to undersampling in space, which needs to be considered when estimating the electric field. Finally, we propose to present the result as a novel 2D contour plot with a high temporal and spatial resolution, with the two plot axis *time* and *esophageal depth*, which inherently emphasizes timing relations between the different channels and along the esophageal depth; we name this plot an esophageal isopotential map (IPM) [4]. An illustrative example of such an esophageal IPM is given in Fig. 1.

This paper is structured as follows: In Section II, we first introduce the idea on how to solve the problems of spatial undersampling and catheter motion. Then, Section III gives an algorithm to estimate the catheter displacement and Section IV an algorithm to estimate the projected electric field in the esophagus, using the catheter displacement estimate. Finally, in Section V, we introduce the graphical IPM and give in Section VI real world examples using records from a clinical trial involving healthy subjects and patients with cardiac arrhythmias.

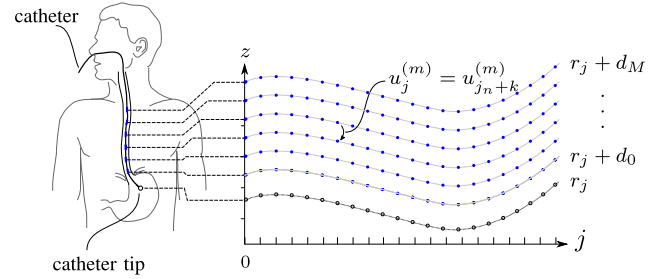


Fig. 3. Illustration of the catheter displacement over time. The catheter contains  $M + 1$  electrodes, located at distances  $d_0, d_1, \dots, d_M$  from the catheter tip, resulting in  $M$  independent measuring channels. The catheter drifts along the  $z$ -axis inside the esophagus. The displacement  $r_j$  (black circles) is the time-dependent position of the catheter tip and  $r_j + d_m$ ,  $m \in \{1, \dots, M\}$  the time-dependent position of the  $m$ th electrode at time index  $j$ . The measurement  $u_j^{(m)}$  is the voltage between electrode “ $m$ ” and “ $m - 1$ ” (small blue dots).

## II. THE BASIC CONCEPT

Common esophageal catheters have a wide electrode spacing, leading to a spatial undersampling of the field along the esophagus. Furthermore, the electrodes are constantly drifting along the esophagus and, in turn, moving with respect to the heart.

By serendipity, solving the tracking problem will help to solve the undersampling problem: The catheter's arbitrarily drifting back and forth along the esophagus axis results in a spatial sampling with small but “randomly” varying changes of the electrode positions. As almost any ECG signal of physiologic or pathologic heart rhythms exhibit some repetitive signal patterns (e.g. repetitive atrial or ventricular waves),<sup>1</sup> we can synchronize between multiple heart beats and, finally, refine the spatial resolution by fusing these beats using an appropriate estimate of the catheter drift. We assume that the start and the length of each such pattern repetition is known and given, e.g. as the result of some prior pattern detection method (which is not part of this paper). An example of a multi-channel EECG is shown in Fig. 2.

We are going to estimate in a first step the movement of the catheter relative to the heart, and use in a second step the estimated movement to extract the catheter and the electrode positions at each heart cycle. This procedure results in spatial sampling along the esophagus axis with small but arbitrary changes in the measuring positions, and thus enhances the spatial resolution. The estimation of the catheter displacement uses the multi-channel record of the current heart beat, allowing various shifts along the esophagus axis, and compares them to the previous heart beat, taking that shift giving the best match between the two beats [5]. This concept is extended and applied to all combinations of heart beats within a selected time frame.

## III. CATHETER DISPLACEMENT RECONSTRUCTION

### A. Definitions

We assume a catheter to be in straight line with the esophagus and to hold  $M + 1$  ring electrodes located at dis-

<sup>1</sup>There exist some medical emergency cases with rhythms showing no repetitive patterns. As these situations are time-critical, the insertion of an esophageal catheter is anyhow not the method of choice.

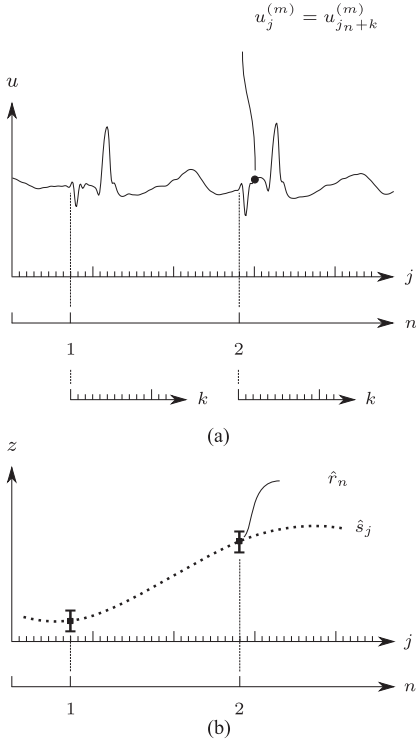


Fig. 4. Illustrative summary of indices and axes subsequently used: (a) single ECG measurement  $u_j^{(m)}$  (black dot), from the  $m$ th measurement channel, with absolute sample time index  $j$ , pattern repetition index  $n = 2$ , and relative per-pattern sample index  $k$ ; (b) catheter displacement estimate  $\hat{r}_n$  for the pattern with index  $n$  and the per-sample interpolation  $\hat{s}_j$ .

tances  $d_0 < d_1 < \dots < d_M$  from the catheter tip. At any given time index  $j \in \{1, \dots, J\}$ ,  $J \in \mathbb{N}$ , we denote  $u_j^{(m)} \in \mathbb{R}$ ,  $m \in \{1, \dots, M\}$ , the potential between the two adjacent electrodes “ $m$ ” and “ $m - 1$ ” (see Fig. 3). Within these  $J$  samples, we observe  $N \in \mathbb{N}$  pattern repetitions with known starting time indices  $j_n \in \mathbb{N}$ ,  $n \in \{1, \dots, N\}$ . Each such pattern repetition is of constant length  $K \in \mathbb{N}$  (cf. Fig. 4(a)) and with unknown catheter displacements  $r_n \in \mathbb{R}$ , which we want to estimate (cf. Fig. 4(b)). The catheter displacement  $r_n$  is referenced as the position of the catheter tip. As we only have relative positions, we fix the catheter displacement of the first pattern repetition to  $r_1 = 0$ .

In the following, we continuously introduce new symbols and indices wherever they are needed. To help the reader to keep track of them, we provide, beside illustrative figures, a summary in Table I.

### B. The Cost Function

We want to estimate the catheter displacement  $r = [r_1, \dots, r_N]$ . For that, we take each pair of repetitive patterns and consider the least square error between the two multi-channel signals with respect to their vertical displacement; to allow a continuous displacement between the two patterns we introduce a function interpolating in between the single channels. Let  $\varphi_j(z)$ ,  $z \in [d_0, d_M]$  be a polynomial of order  $N_\varphi < M$  approximating and interpolating the measurements  $(u_j^{(1)}, \dots, u_j^{(M)})$ .

TABLE I  
SUMMARY OF RELEVANT SYMBOLS AND INDICES

Symbol	Range	Description
<b>Scalar Indices</b>		
$m$	$\{1, \dots, M\}$	measuring channel index
$j$	$\{1, \dots, J\}$	absolute sample/time index
$k$	$\{1, \dots, K\}$	relative per-pattern sample/time index
$n$	$\{1, \dots, N\}$	pattern repetition index
$i$	$\{\dots, 0, 1, 2, \dots\}$	position index along the $z$ -axis/esophagus
$j_n$	$\{1, \dots, J\}$	sample/time start index of $n$ th pattern repetition, $n \in \{1, \dots, N\}$
<b>Vectors, Functions, and Others</b>		
$d_0, \dots, d_M$	$\mathbb{R}^+$	electrode distance from catheter tip position along the $z$ -axis/esophagus
$z$	$\mathbb{R}$	polynomial interpolation function of $(u_j^{(1)}, \dots, u_j^{(M)})$ at $j$ ; $z \in [d_0, d_M]$
$u_j^{(m)}$	$\mathbb{R}$	measured voltage on channel “ $m$ ” at time index $j$
$\varphi_j(z)$	$\mathbb{R}$	polynomial interpolation function of $(u_j^{(1)}, \dots, u_j^{(M)})$ at $j$ ; $z \in [d_0, d_M]$
$r = [r_1, \dots, r_N]$	$\mathbb{R}^N$	true relative catheter displacement per pattern repetition; $r_1 = 0$
$\hat{r} = [\hat{r}_1, \dots, \hat{r}_N]$	$\mathbb{R}^N$	estimate of $r$
$\hat{s} = [\hat{s}_1, \dots, \hat{s}_J]$	$\mathbb{R}^J$	estimate of catheter (tip) displacement per sample; $\hat{s}_j = \hat{s}(j)$
$\hat{s}_j^{(m)}$	$\mathbb{R}$	per sample displacement estimate of the center between electrodes “ $m$ ” and “ $m - 1$ ”
$\hat{s}(t)$ , $t \in \mathbb{R}$	$\mathbb{R}$	continuous-time estimate of catheter displacement
$q(z)$	$\mathbb{R}$	true (projected) electric field along the $z$ -axis
$\hat{q}_i$	$\mathbb{R}$	estimate of $q(z)$ at position index $i$ (per relative sample index $k$ )

We define the cost function to compare a pair of patterns with indices  $n \in \{1, \dots, N\}$  and  $\nu \in \{1, \dots, N\}$  with the displacement  $\rho \in \mathbb{R}$  by computing the squared error,

$$R_{n,\nu}(\rho) = \sum_{k=0}^K \int_{-\infty}^{\infty} [\varphi_{j_n+k}(z) - \varphi_{j_\nu+k}(z - \rho)]^2 \times \delta_{[d_0, d_M]}(z) \delta_{[d_0, d_M]}(z - \rho) dz, \quad (1)$$

with  $\delta_{[a,b]} : \mathbb{R} \rightarrow \{0, 1\}$ ,  $a \in \mathbb{R}$ ,  $b \in \mathbb{R}$ ,  $a < b$  and  $\delta_{[a,b]}(r) = 1$  for  $a \leq r < b$  and  $\delta_{[a,b]}(r) = 0$  otherwise. This pairwise cost  $R_{n,\nu}$  of (1) is a piecewise polynomial in  $\rho$  and also writes as

$$R_{n,\nu}(\rho) = \sum_{k=0}^K \begin{cases} \int_{d_0+\rho}^{d_M} [\varphi_{j_n+k}(z) - \varphi_{j_\nu+k}(z - \rho)]^2 dz & \text{if } 0 \leq \rho < d_M - d_0, \\ \int_{d_0}^{d_M+\rho} [\varphi_{j_n+k}(z) - \varphi_{j_\nu+k}(z - \rho)]^2 dz & \text{if } d_0 - d_M \leq \rho < 0, \\ 0 & \text{otherwise.} \end{cases} \quad (2)$$

Since not only do we need to compare and optimize between a single pair but also over all possible pairs, we get an over-all

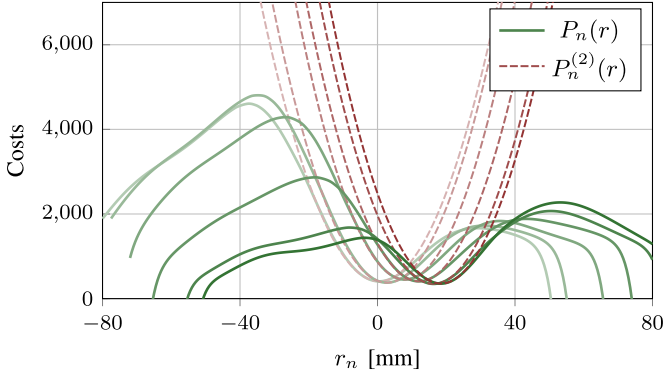


Fig. 5. Illustrative examples of costs  $P_n(r)$  from (3) as a function of  $r_n$  (green, solid lines). The order of the interpolating polynomials  $\varphi_j(\cdot)$  is set to  $N_\varphi = 7$ , resulting in piecewise polynomials  $P_n(r)$  of order 15 (cf. (3) and (1)). Additionally given are the local quadratic approximations  $P_n^{(2)}(\cdot)$  with parameters from (10) over the range  $[r_n - \delta, r_n + \delta]$  with  $\delta = 5$  mm for each cost function (red, dashed lines).

cost function

$$P(r) = \sum_{n=1}^N \underbrace{\sum_{\nu=1}^N R_{n,\nu}(r_\nu - r_n)}_{P_n(r)}, \quad (3)$$

where  $r$  is the introduced vector of catheter displacements. Using the symmetry property  $R_{n,\nu}(\rho) = R_{n,\nu}(-\rho)$  and the trivial property  $R_{n,\nu}(0) = 0$ , we get

$$P(r) = 2 \sum_{n=1}^{N-1} \sum_{\nu=n+1}^N R_{n,\nu}(r_\nu - r_n). \quad (4)$$

Fig. 5 illustrates some example cost polynomials  $P_n(r)$ .

### C. Cost Minimization by Gradient Descent

To minimize (3), we use the method of gradient descent. Since physics prohibits position jumps, we also add a regularization term for  $r$ ,

$$S(r) = \mu_0 \sum_{n=1}^{N-1} \sum_{\nu=n+1}^N \frac{(r_n - r_\nu)^2}{j_n - j_\nu} \in \mathbb{R}^+, \quad (5)$$

with single parameter  $\mu_0 \in \mathbb{R}^+$ , controlling the smoothness of the displacement estimate. We get

$$\hat{r} = \underset{r}{\operatorname{argmin}} (P(r) + S(r)). \quad (6)$$

To solve, we iterate for  $r$  with

$$r^{(\text{new})} = r^{(\text{old})} - \gamma \nabla (P(r^{(\text{old})}) + S(r^{(\text{old})})) \quad (7)$$

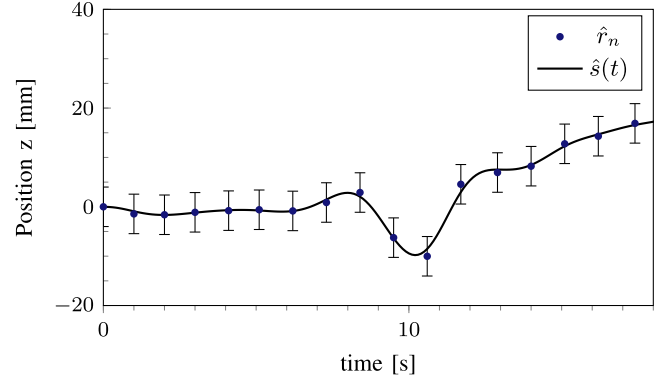


Fig. 6. Example of catheter displacement estimate from an ECG of a healthy subject. Shown are: displacement  $\hat{r}_n$  at each heart beat (blue dots), Variances  $\sigma_n^2$  from (10) of the quadratic approximation (vertical error bars) and displacement interpolation using the Kalman smoother  $\hat{s}(t)$  (solid black line).

with the gradient operator  $\nabla$  and with step size  $\gamma \in \mathbb{R}^+$ . The derivative for  $r_n$  from (7) is

$$\frac{\partial (P(r) + S(r))}{\partial r_n} = \sum_{\substack{\nu \in \{2, \dots, N\} \\ \setminus \{n\}}} \frac{\partial}{\partial r_n} R_{j_n, j_\nu}(r_\nu - r_n) + 2\mu_0 \frac{(r_n - r_\nu)}{j_n - j_\nu}. \quad (8)$$

Recall that  $R_{j_n, j_\nu}(\rho)$  is a continuous, piecewise polynomial in  $\rho$  and thus, its piecewise derivative is simply obtained. However, its first derivative is not defined at the points between the pieces (i.e.,  $\rho \in \{-d_M, 0, d_M\}$ ). Nevertheless, in practice, sufficient convergence was still observed using the derivative at  $\rho^+$  (or  $\rho^-$ ) instead. Furthermore, note that (3) is not necessarily convex (cf. Fig. 5). But since it is sufficient to find that local minimum with only small relative displacements between neighboring patterns, this is not a necessary condition. As a positive side effect, outliers are easily detected (and discarded) during the gradient iterations, as displacement estimates of invalid patterns usually tend to diverge, rather than to converge to a local cost minimum, or to converge to a minimum but with a large cost remainder.

An example of the estimated pattern-wise catheter displacement after applying gradient descent is given in Fig. 6.

### D. Catheter Displacement Interpolation Using a Kalman Smoother With Weighted Samples

In the previous Section III-C, we computed a catheter displacement estimate for every pattern repetition, which occur with a *variable* time delay. To gain smooth displacement estimates on an equidistant time grid, we use a Kalman smoother [6], [7], which is capable to transform between different time grids.<sup>2</sup> For that, we introduce the auxiliary *continuous-time* catheter displacement estimate  $s(t) \in \mathbb{R}$ ,  $t \in \mathbb{R}$ , and the *continuous-time* cost function, parameterized by sample mean

<sup>2</sup>We chose a Kalman smoother as we have wide experiences with the parameterization of this kind of filters; there are surely other methods to obtain results of comparable quality.

$m_n \in \mathbb{R}$  and sample variance  $\sigma_n^2 \in \mathbb{R}^+$ ,  $n \in \{1, \dots, N\}$ ,

$$\hat{s}(t) = \underset{s(t)}{\operatorname{argmin}} \sum_{n=1}^N \sigma_n^{-2} (s(j_n) - m_n)^2 + \mu_0 \int_0^J \left( \frac{d^2 s(t)}{dt^2} \right)^2 dt. \quad (9)$$

We are only interested in  $\hat{s}(t)$  on the equidistant time grid  $t \in \{1, \dots, J\}$ ; thus, we denote the outcome as  $\hat{s} = [\hat{s}_1, \dots, \hat{s}_J]$  with  $\hat{s}_j = \hat{s}(j)$ . The sample mean  $m_n$ , sample variance  $\sigma_n^2$  and in addition the offset  $\kappa_n \in \mathbb{R}$  are a local quadratic approximate  $P_n^{(2)}(\cdot)$  of  $P_n(\cdot)$  from (3) for the  $n$ th pattern repetition, i.e.,

$$\{m_n, \sigma_n^2, \kappa_n\} = \underset{m, \sigma^2, \kappa}{\operatorname{argmin}} \int_{\hat{r}_n - \delta}^{\hat{r}_n + \delta} \left[ \sigma^{-2} (\rho - m)^2 + \kappa - P_n([\hat{r}_1, \dots, \hat{r}_{n-1}, \rho, \hat{r}_{n+1}, \dots, \hat{r}_N]) \right]^2 d\rho, \quad (10)$$

with  $\delta \in \mathbb{R}^+$  selected sufficiently small (see Fig. 5). For efficient minimization of (9), we use the Kalman Smoother with the Modified Bryson-Frazier Message Passing scheme from Bruderer *et al.* [8], modified to deal with weighted samples. The filter is given by the linear state space system matrices

$$\begin{aligned} A &= \begin{bmatrix} 1 & 0 & 0 \\ 1 & 1 & 0 \\ 0 & 1 & 1 \end{bmatrix} \\ B &= [1 \quad 0 \quad 0]^\top \\ C &= [0 \quad 0 \quad 1], \end{aligned} \quad (11)$$

representing a second-order integrator chain and is equivalent to (9) (cf. Theorem 2 in [9]). The filter runs recursively forward and backward over index  $j \in \{1, \dots, J\}$  and is fed with observations of Gaussian distribution  $\mathcal{N}(m_n, \sigma_n^2/w_j)$  with sample weight  $w_j = 1$  for  $j = j_n$  and  $\mathcal{N}(0, 1)$  with sample weight  $w_j = 0$  in all other cases, where we have no sample.

The interpolated catheter displacement results as  $\hat{s}_j = C m_{x_j}$  with  $m_{x_j}$  being the posterior mean state vector of the LSSM (11). The filter's full computation rules are summarized in Appendix A. An example of an interpolated catheter displacement estimate is given in Fig. 6.

## IV. ELECTRIC FIELD RECONSTRUCTION

### A. Introduction

In the previous section we determined the per-pattern estimate of the catheter displacement  $\hat{r}_n$ ,  $n \in \{1, \dots, N\}$  and also, using interpolation, the per-sample displacement  $\hat{s}_j$ ,  $j \in \{1, \dots, J\}$ . We note that  $\hat{r}_n$  and  $\hat{s}_j$  both refer to the position of the catheter tip (not to that of a particular electrode).

Now, we want to estimate the electric field at any relative time index  $k$  in such a way, that the catheter displacement is taken into account. (Recall that  $k$  is the relative time index within a single pattern, see Fig. 4(a).) To do so, we assume the catheter to be in a straight line coinciding with the  $z$ -axis (cf. Fig. 3) and

denote the electric field along the  $z$ -axis as  $q(z) \in \mathbb{R}$  for  $z \in \mathbb{R}$  (i.e. the projection of the field to the  $z$ -axis).

Considering first any potential difference  $u(z) \in \mathbb{R}$  measured between 2 adjacent ring electrodes located at distances  $d_0$  and  $d_1$  from the catheter tip and a catheter insertion depth of  $z \in \mathbb{R}$ . If the distance  $d_1 - d_0$  is sufficiently small, we could approximate the electric field by

$$q\left(z + \frac{d_0 + d_1}{2}\right) \approx \frac{u(z)}{d_1 - d_0}. \quad (12)$$

However, as discussed in Section I, for common catheters the electrode distances are rather large and the approximation (12) turns out to be inadequate. Therefore we need to consider the integral of the (projected) electric field  $q(z)$ , i.e.,

$$u(z + d_1) = p(z + d_1) - p(z + d_0) \quad (13)$$

with the absolute electric potential

$$p(z) = \int_{-\infty}^z q(\rho) d\rho \in \mathbb{R}. \quad (14)$$

### B. Estimation

We recall that the sequence  $(u_1^{(m)}, \dots, u_J^{(m)})$  is a single-channel esophageal ECG signal of  $J$  samples<sup>3</sup> measured between the electrodes “ $m$ ” and “ $m - 1$ ” with estimated catheter tip insertion depth  $\hat{s} = [\hat{s}_1, \dots, \hat{s}_J]$  from Section III-D. We also note that the measurement  $u_{j_n+k}^{(m)} \in \mathbb{R}$  corresponds to the  $k$ th sample of the  $n$ th pattern repetition on the  $m$ th channel (cf. Fig. 4(a)). Accordingly we denote  $\hat{s}_{j_n+k}^{(m)} = \hat{s}_{j_n+k} + \frac{1}{2}(d_m + d_{m-1})$  the average insertion depth of the two electrodes involved.

We now join the measurements of all pattern repetitions with the same relative time index  $k$  and sort them according to their electrode insertion depth. We sort them to multiple bins  $\Omega_i^{(k)}$ ,  $i \in \{\dots, -1, 0, 1, 2, \dots\}$ , each bin spanning over a single, non-overlapping interval of length  $\lambda \in \mathbb{R}^+$  on the  $z$ -axis, i.e.:

$$\Omega_i^{(k)} = \left\{ u_{j_n+k}^{(m)} \mid i \cdot \lambda - \frac{\lambda}{2} \leq \hat{s}_{j_n+k}^{(m)} < i \cdot \lambda + \frac{\lambda}{2}, m \in \{1, \dots, M\}, n \in \{1, \dots, N\} \right\}. \quad (15)$$

Note that a lower value of parameter  $\lambda$  increases the maximal spatial resolution on the  $z$ -axis, but also increases the computational effort; we found for our examples that  $\lambda = 0.1$  mm is an appropriate value. Fig. 7 illustrates the re-ordering process according to the bin intervals. For later use, we extract for each non-empty bin the cardinality  $w_i^{(k)}$  and the empirical mean  $m_i^{(k)}$ , i.e.,

$$w_i^{(k)} = |\Omega_i^{(k)}| \quad (16)$$

$$m_i^{(k)} = \frac{1}{w_i^{(k)}} \sum_{u \in \Omega_i^{(k)}} u, \quad (17)$$

or set  $w_i^{(k)} = 0$  and  $m_i^{(k)} = 0$  for any empty bin.

<sup>3</sup>We assume a sufficiently large (temporal) sampling rate of the recordings such that the assumptions of the Nyquist-Shannon sampling theorem hold.

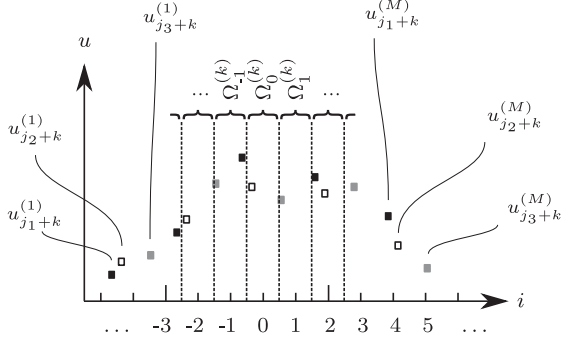


Fig. 7. Illustration of the bins  $\Omega_i^{(k)}$ ,  $i \in \{\dots, -1, 0, 1, 2, \dots\}$ , for a single relative time index  $k$ . Each bin contains the measurements with similar electrode position estimates  $\hat{s}_{j_n+k}^{(m)}$  over multiple pattern repetitions  $n \in \{1, \dots, N\}$ , all with equal relative time index  $k$ . The small squares display example multi-channel measurements  $(u_j^{(1)}, \dots, u_j^{(M)})$  of three pattern repetitions with absolute time indices  $j_1 + k$  (black squares),  $j_2 + k$  (white squares) and  $j_3 + k$  (grey squares).

To finally estimate, based on the sorted measurements, the fundamental electric field (for any particular relative time index  $k$ ), we consider (13) as a linear filter, which we are going to discretize with respect to continuous position  $z$ , and design the filter in the  $z$ -domain. For the sake of simplicity, we use the bin size  $\lambda$  also as the discretization grid distance.

Let  $Q_k(z)$  be the  $z$ -transform of a discretized electric field  $q(z)$  and  $U_k(z)$  the  $z$ -transform of discrete samples of a continuous measurement  $u(z) \in \mathbb{R}$ , both with respect to position  $z$  (and not to time index  $k$ ), and let  $\Delta \in \mathbb{N}$  be the (discrete) electrode distance. Then the  $z$ -transform of (13) writes as

$$U_k(z) = G(z)Q_k(z) \quad (18)$$

with

$$G(z) = \lambda \cdot (1 - z^{-\Delta}) \frac{z}{z - 1}. \quad (19)$$

(At this point,  $z \in \mathbb{C}$  is the  $z$ -transform variable and is not to be confused with the  $z \in \mathbb{R}$ , the position on the  $z$ -axis.) As the inverse  $G^{-1}(z)$  is not a stable filter, we use a Kalman filter [10] with an additional regularization term to estimate the electric field  $Q_k(z)$  as the input to  $G(z)$ , given the observations  $U_k(z)$ . The regularization term will assure stability of the filter inverse. We again use the Kalman filter summarized in Appendix A with two joined LSSM, such that the output of the first system is fed as the input to the second system; the first system with parameters  $\{B_1, A_1, C_1\}$  is the regularization term, in our case a 2nd order integrator chain, the second system with parameters  $\{B_2, A_2, C_2\}$  the transfer function (19) in its controllable form. The input of the first system is an (assumed) zero-mean Gaussian input, leading to a stable filter inverse [11], as recently used in [12]. The first system  $\{B_1, A_1, C_1\}$  writes as in (11), the second

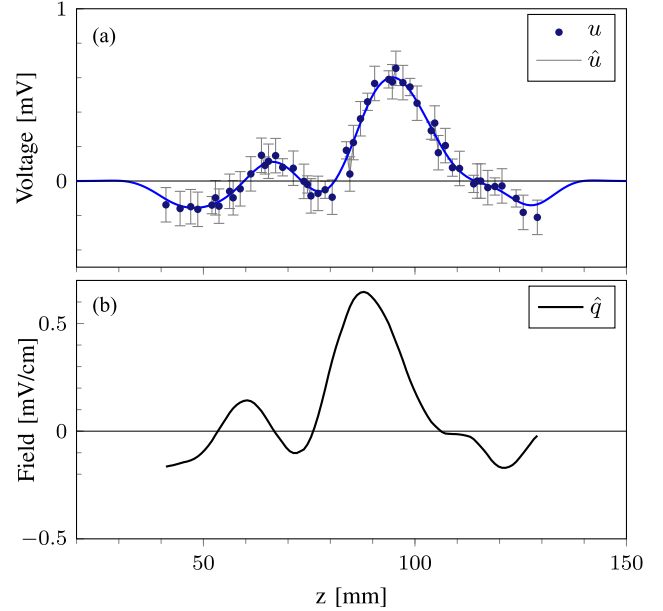


Fig. 8. Example of electric field estimate using Kalman filtering at a particular sample index  $k = 47$ . (a) Joined measurements at a particular sample index  $k$  over all the recorded pattern repetitions, leading to non-equidistant samples along the  $z$ -axis. Each sample consists of the mean  $m_i^{(k)}$  (black dots) and the variance  $1/w_i^{(k)}$  (vertical error bars) of a single bin  $\Omega_i^{(k)}$ ,  $i \in \{\dots, -1, 0, 1, 2, \dots\}$ . The measurements are superimposed by the continuous input estimate from the Kalman filter (blue line). (b) Electric field estimate.

system as

$$A_2 = \left[ \begin{array}{cccc|c} 1 & 0 & \dots & 0 & 0 \\ & 1 & & & \vdots \\ & & \ddots & & \vdots \\ & & & \ddots & \vdots \\ & & & & 1 & 0 \\ \hline 0 & \dots & \dots & 0 & 0 & 0 \end{array} \right] \quad (20)$$

$$B_2 = [1 \ 0 \ \dots \ 0 \ | \ 1]^T$$

$$C_2 = \left[ \underbrace{0 \ \dots \ 0}_{\Delta} \ 1 \ | \ -1 \right],$$

and, finally, the joined LSSM is

$$A = \left[ \begin{array}{c|c} A_1 & 0 \\ \hline B_2 C_1 & A_2 \end{array} \right]$$

$$B = \left[ \begin{array}{c} B_1 \\ 0 \end{array} \right] \quad (21)$$

$$C = [0 \ | \ C_2].$$

The filter runs recursively forward and backward over the bin index  $i$  (and not over the relative time index  $k$ ), and is fed with observations of Gaussian distribution  $\mathcal{N}(m_i^{(k)}, 1/w_i^{(k)})$  for non-empty bins, and with  $\mathcal{N}(0, 1)$  and weight  $w_i^{(k)} = 0$  for all

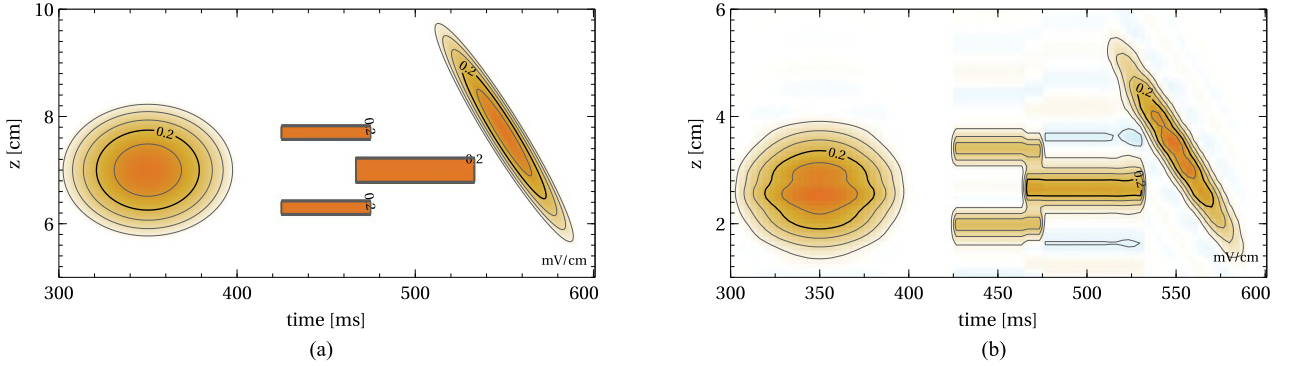


Fig. 9. Verification of the algorithm using a synthetic electric field containing abrupt changes in the field strength. (a) Contour plot of synthetic “true” electric field. (b) IPM of electric field using our reconstruction algorithm. The “true” field was sampled with a 9 channel catheter with an electrode distance of 1 cm. Note that the  $z$ -axis is scaled differently from other IPM figures.

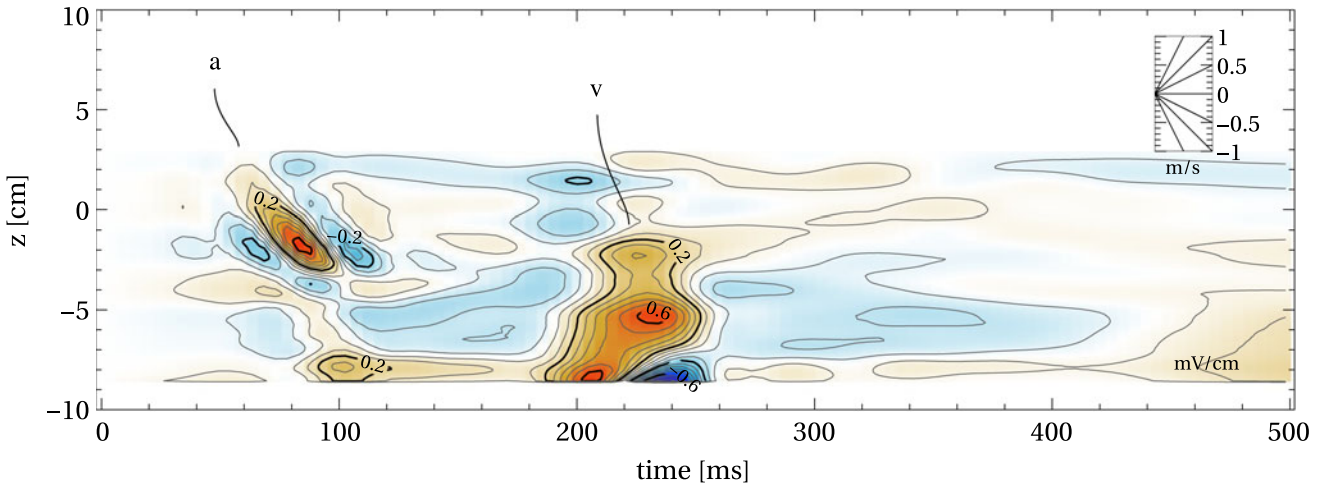


Fig. 10. IPM of a healthy 59 years old male. Atrial wave (a), ventricular wave (v).

empty bins. The Kalman filter outputs an estimate of Gaussian distribution with mean  $m_{x_i}$  and variance  $V_{x_i}$ . Subsequently, the electric field results as  $\hat{q}_i = C_0 m_{x_i}$  with variance  $C_0 V_{x_i} C_0^T$ , using the selection vector  $C_0 = [C_1 \mid 0]$ .

An example of such a field estimate at a particular index  $k$  is given in Fig. 8.

## V. THE ESOPHAGEAL ISOPOTENTIAL MAP

We introduce a new graphical representation of the field estimated in the previous section. We name this representation the *esophageal isopotential map* (IPM) [4]. An example of such an IPM is shown in Fig. 1. An IPM is the spatiotemporal representation of the projected cardiac electric field measured in the esophagus, depicted as a 2D contour plot with *time* on the horizontal axis (abscissa), the *esophageal location* on the vertical axis (ordinate), and the electric field projection depicted as contour levels. For the electric field we propose to use the unit 1 mV/cm, leading to convenient and meaningful numeric values. The contours are open or closed curves along which the electric field has constant values. The contour level spacing is fixed to a constant value, e.g. to 0.20 mV/cm.

## VI. RESULTS

Fig. 9(a) shows a synthetic field test pattern and Fig. 9(b) the corresponding estimate after reconstruction of that field using the proposed algorithm. The purpose of this reconstruction of the known test field is to give to the reader an intuitive access to the reconstruction efficiency of the proposed algorithm. The chosen test pattern deliberately deviates from an esophageal electric field: it contains abrupt changes in the field strength in order to identify the limits of the algorithm. The reconstruction bases on a 9 channel synthetic EECG signal, recorded using an equidistant electrode spacing of 1 cm and with a slowly varying catheter displacement. The comparison of the estimate to the reference signal reveals some blurring and smoothing artifacts introduced by the algorithm: this is, along the time axis, essentially due to the low pass filtering applied to all EECG signals (in order to suppress the omnipresent baseline interferences [13]) and along the  $z$ -axis due to the smoothing effect of the regularization term in the Kalman filter (Section III-D).

To show the suitability of our method, we performed a clinical trial with 13 patients and 6 healthy subjects. From each participant, we recorded about 1 hour of EECG signals using a commercially available 9 channel catheter (*Esoflex 10S*, *FIAB*

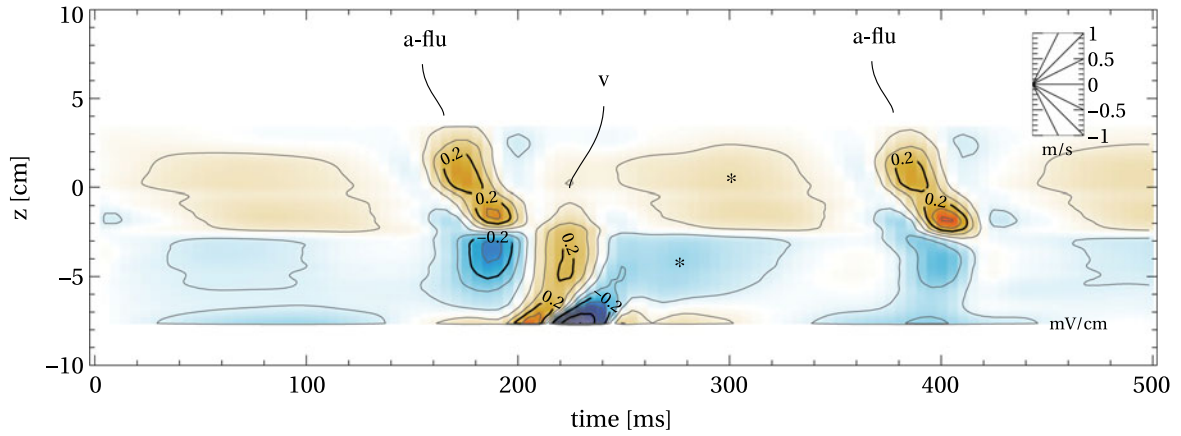


Fig. 11. IPM of a 67 years old patient with typical counterclockwise atrial flutter: atrial flutter waves (a-flu), ventricular wave (v), high pass filter artifacts (\*).

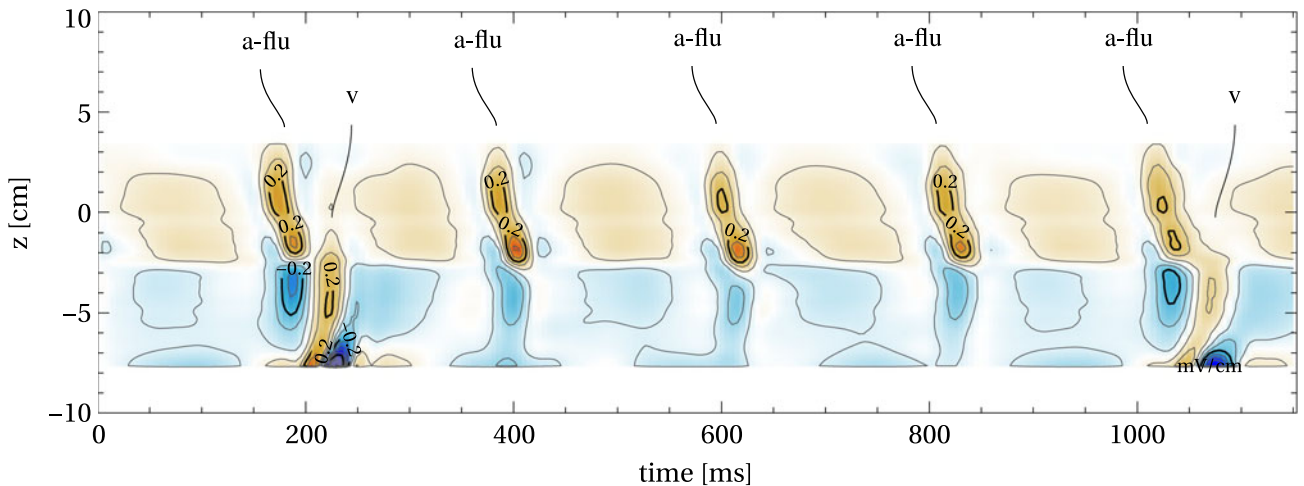


Fig. 12. IPM as in Fig. 11 but with time axis spanning 1200 ms to emphasize the heart rhythm (counterclockwise atrial flutter with 4:1 conduction from the atrium to the ventricle): atrial flutter waves (a-flu), ventricular waves (v).

SpA, Italy) with an electrode spacing of 1 cm. The signals were recorded with *g.USBamp* (*g.tec medical engineering GmbH, Austria*) at a sampling frequency of 4800 Hz. All esophageal channels were initially filtered with an IIR high-pass filter, applied in forward and backward direction to prevent phase distortion. The IIR filter is implemented as a second order Butterworth filter with a cut-off frequency of 1 Hz.

Fig. 10 shows an exemplary IPM of a healthy subject. The atrial and ventricular signals are of high resolution and the propagation direction along the  $z$ -axis is clearly visible. Figs. 11 and 12 show IPMs of a patient with typical counterclockwise atrial flutter. The atrial signal with its high repetition rate is immediately apparent and the propagation direction of each atrial flutter wave is again directly read from the plot. To interpret this IPM example, we have to keep in mind that the esophageal electric field is dominated by the cardiac activity located in close proximity to the esophagus, i.e., by activity located in the left atrium. Thus, we here mainly observe the left atrial part of the flutter wave.

The two examples shown well demonstrate the qualities of esophageal IPMs: the plots are of high atrial resolution and inherently emphasize the spatial location of the cardiac activity

(with respect to the  $z$ -axis), and finally immediately visualize the propagation directions. The clinical value and benefit of IPMs are further discussed and illustrated with multiple examples in [14] and [15]. A next clinical trial is already approved by the authorities and ready to start.

## VII. CONCLUSION

In this paper, we have presented a novel approach to estimate the catheter displacement and to increase the spatial resolution of esophageal ECG measurements for a medical applications, taking advantage of the particular nature of the signal. As we have shown in Section VI, this approach is ready to work with clinical data, recorded with commonly available equipment. However, its value as a complementary diagnostic tool in the arrhythmia diagnostics needs to be prospectively evaluated. The output representation of this method, the IPMs, were already presented in [14] and [15] and need additional clinical trials to be further evaluated.

To summarize the presented algorithm, it splits the initial problem into multiple consecutive processing steps and makes use of versatile quadratic and more elaborate cost functions

defined in the time, as well as in the spatial domain. The output of each step (except the last) is not a point estimate, but a cost function that can be processed by the subsequent step. In this way, the loss of information in each processing step is reduced. For example, in Section III-D, we use a Kalman smoother to re-map the non-equidistant depth estimation to an equidistantly sampled representation. We use not only quadratic cost functions, but also higher order polynomials, both over time and over space, as illustrated in Fig. 5.

## APPENDIX A

### KALMAN SMOOTHER WITH MODIFIED BRYSON-FRAZIER MESSAGE PASSING SCHEME

There are different methods to compute Kalman filters; one method is the Modified Bryson-Frazier message passing scheme [11], which avoids matrix inversions, and thus is computationally highly efficient in solving many filtering tasks. In the following, we give a full summary of the recursive computation rule for such a filter processing scalar observations (modified from Bruderer *et al.* [8] to work with weighted samples). This Kalman filter is based on linear state space models (LSSM) of order  $N \in \mathbb{N}$  and is parametrized by *discrete time state matrix*  $A \in \mathbb{R}^{N \times N}$ , *output vector*  $C \in \mathbb{R}^{1 \times N}$ , *observation noise variance*  $\sigma_{Z,k}^2 \in \mathbb{R}^+$ , and *input variance*  $\sigma_U^2 \in \mathbb{R}^+$ . The filter is fed with observations of Gaussian distribution, i.e.,  $\mathcal{N}(m_{y_k}, \sigma_{Z,k}^2)$  for  $k \in \{1, \dots, K\}$ ,  $K \in \mathbb{N}$ , each with its *sample weight*  $w_k$ . We extend the filter by that sample weight  $w_k \in \mathbb{R}_0^+$ , allowing to weight each sample differently. For our application, the special case  $w_k = 0$  is of particular importance, whenever there is no sample for a single index  $k$ .

To perform the filtering, the Gaussian distribution of the LSSM *state vector*  $x \in \mathbb{R}^{N \times 1}$  with mean vector  $m_{x_k} \in \mathbb{R}^{N \times 1}$  and covariance matrix  $V_{x_k} \in \mathbb{R}^{N \times N}$ , is efficiently computed using recursions: the forward recursion for  $k = 1, \dots, K$  follows as

$$G_k = w_k \left( \sigma_{Z,k}^2 + w_k C \vec{V}_{x_k}'' C^T \right)^{-1} \quad (22)$$

$$F_k = \mathbb{I} - \vec{V}_{x_k}'' C^T G_k C \quad (23)$$

$$\vec{V}_{x_k}'' = A \vec{V}_{x_{k-1}} A^T + \Sigma \quad (24)$$

$$\vec{m}_{x_k} = A \vec{m}_{x_{k-1}} + \vec{V}_{x_k}'' C^T G (m_{y_k} - C A \vec{m}_{x_{k-1}}) \quad (25)$$

$$\vec{V}_{x_k} = \vec{V}_{x_k}'' - \vec{V}_{x_k}'' C^T G C \vec{V}_{x_k}'' \quad (26)$$

with  $\mathbb{I}$  denoting the unity matrix, the variance update

$$\Sigma = \sigma_U^2 \int_0^{T_s} e^{A\tau} b b^T e^{A^T \tau} d\tau \quad (27)$$

with  $T_s = 1$ , and with  $\vec{V}_{x_0}''$ ,  $\vec{m}_{x_0}$ , and  $\vec{V}_{x_0}$  all initialized to zero. The backward recursion for  $k = K, \dots, 1$  follows as

$$\tilde{\xi}_{x_k} = A^T \left( F_k^T \tilde{\xi}_{x_{k+1}} + C^T G_k (C A \vec{m}_{x_{k-1}} - m_{y_k}) \right) \quad (28)$$

$$\tilde{W}_{x_k} = A^T \left( F_k^T \tilde{W}_{x_{k+1}} F_k + C^T G_k C \right) A, \quad (29)$$

with  $\tilde{\xi}_{x_{K+1}}$  and  $\tilde{W}_{x_{K+1}}$  initialized all to zero. Finally, this computations lead to a *state vector* of Gaussian distribution with mean and variance

$$m_{x_k} = \vec{m}_{x_k} - \vec{V}_{x_k} \tilde{\xi}_{x_k} \quad (30)$$

$$V_{x_k} = V_{x_k} (\mathbb{I} - \tilde{W}_{x_k} V_{x_k}). \quad (31)$$

The distribution of the final (scalar) signal of interest is extracted from the *state vector*, using the selection matrix  $C_0 \in \mathbb{R}^{1 \times N}$  and follows as  $\mathcal{N}(C_0 m_{x_k}, C_0 V_{x_k} C_0^T)$ .

## ACKNOWLEDGMENT

All EECG signals presented were recorded during a collaborative clinical trial at the Bern University Hospital. The trial was approved by the swiss ethics commission, No. 149/15 (Clinical-Trials.gov/NCT02541175).

## REFERENCES

- [1] M. N. Benzadon *et al.*, "Comparison of the amplitude of the p-wave from intracardiac electrocardiogram obtained by means of a central venous catheter filled with saline solution to that obtained via esophageal electrocardiogram," *Amer. J. Cardiology*, vol. 98, no. 7, pp. 970–981, 2006.
- [2] T. Niederhauser, T. Marisa, A. Haerberlin, J. Goette, M. Jacoment, and R. Vogel, "High-resolution esophageal long-term ECG allows detailed atrial wave morphology analysis in case of atrial ectopic beats," *Med. Biol. Eng. Comput.*, vol. 50, no. 7, pp. 769–772, Jul. 2012.
- [3] M. Cremer, "Über die direkte Ableitung der Aktionsströme des menschlichen Herzens vom Ösophagus und über das EKG des Fötens," *Munchener Medizinische Wochenschrift*, vol. 53, pp. 811–813, 1906.
- [4] R. A. Wildhaber, "Apparatus for providing electrocardiographic and especially arrhythmia information," Patent EP17198175.6, Oct. 2017.
- [5] N. Zalmi, R. A. Wildhaber, and H.-A. Loeliger, "Autonomous state space models for recursive signal estimation beyond least squares," in *Proc. 25th Eur. Signal Process. Conf.*, Aug. 2017, pp. 341–345.
- [6] R. E. Kalman and R. S. Bucy, "New results in linear filtering and prediction theory," *J. Fluids Eng.*, vol. 83, no. 1, pp. 95–108, 1961.
- [7] H.-A. Loeliger, L. Bruderer, H. Malmberg, F. Wadehn, and N. Zalmi, "On sparsity by NUV-EM, Gaussian message passing, and Kalman smoothing," in *Proc. Inf. Theory Appl. Workshop*, Jan. 2016, pp. 1–10.
- [8] L. Bruderer, "Input estimation and dynamical system identification: New algorithms and results," Ph.D. dissertation, Dept. Info. Technol. Elect. Eng., No. 22575, ETH Zurich, Zürich, Switzerland, 2015.
- [9] L. Bolliger, H.-A. Loeliger, and C. Vogel, "LMMSE estimation and interpolation of continuous-time signals from discrete-time samples using factor graphs," arXiv:1301.4793v1 [cs.LG], Jan. 2013.
- [10] L. Bruderer and H.-A. Loeliger, "Estimation of sensor input signals that are neither bandlimited nor sparse," in *Proc. IEEE Inf. Theory Appl. Workshop*, 2014, pp. 1–5.
- [11] T. Kailath, A. H. Sayed, and B. Hassibi, *Linear Estimation*, vol. 1. Upper Saddle River, NJ, USA: Prentice-Hall, 2000.
- [12] H.-A. Loeliger, L. Bolliger, G. Wilckens, and J. Biveroni, "Analog-to-digital conversion using unstable filters," in *Proc. 2011 Inf. Theory Appl. Workshop*, Feb. 2011, pp. 1–4.
- [13] T. Niederhauser *et al.*, "Graphics-processor-unit-based parallelization of optimized baseline wander filtering algorithms for long-term electrocardiography," *IEEE Trans. Biomed. Eng.*, vol. 62, no. 6, pp. 1576–1584, Jun. 2015.
- [14] R. Wildhaber *et al.*, "A novel 2-D spatial-temporal ECG representation using multipolar esophageal catheters: A pilot study," *JACC, Clin. Electrophysiol.*, vol. 3, no. 10, Supplement S2, p. 3, Oct. 2017, doi: [10.1016/j.jacep.2017.09.013](https://doi.org/10.1016/j.jacep.2017.09.013).
- [15] S. A. Mortier, "Esophageal isopotential maps, a case series," M.D. dissertation, Dept. Cardiology, Univ. Berne, Bern, Switzerland, to be published.



**Reto Andreas Wildhaber** received the degree in electrical engineering from the University of Applied Science, Rapperswil, Switzerland, in 2003, and the M.Sc. degree in medicine and the M.D. degree, both from the University of Zurich, Zurich, Switzerland, in 2013 and 2014, respectively. He is currently working toward the Ph.D. degree at the Department of Information Technology and Electrical Engineering, ETH Zurich, Zurich, Switzerland. He is with Bern University of Applied Science, Biel, Switzerland, and collaborates with the University Hospital Bern.



**Dominik Bruegger** received the B.Sc. degree in electrical engineering from Bern University of Applied Sciences, Bern, Switzerland, in 2014, and the M.Sc. degree in biomedical engineering from the University of Bern, Bern, Switzerland, in 2016. He is currently working toward the Ph.D. degree at the University Hospital Bern, Bern, Switzerland. His research interests include the application of signal processing techniques to clinical problems.



**Nour Zalmai** received the Electrical Engineering Diploma in 2013 from Supélec, Gif-sur-Yvette, France, and the M.Sc. and Ph.D. degrees in electrical engineering, both from ETH Zurich, Zurich, Switzerland, in 2013 and 2017, respectively.

His research interests include signal processing and graphical models for learning sparse signal decompositions.



**Hampus Malmberg** received the B.Sc. degree in electrical engineering from Chalmers University of Technology, Göteborg, Sweden, in 2012, and the M.Sc. degree in electrical engineering from ETH Zurich, Zurich, Switzerland, in 2014. He is currently working toward the Ph.D. degree in electrical engineering at ETH Zurich.



**Josef Goette** received the Dipl. El. Ing. (M.E.E.) and Dr. sc. techn. (Ph.D.) degree from the Swiss Federal Institute of Technology (ETH), Zurich, Switzerland.

From 1977 to 1982, he did industrial research at the Institute of Applied Physics, ETH. From 1983 to 1994, he was a Research Associate with the Electronics Laboratory, ETH. Since 1992, he has been a Lecturer with the Engineering School of Biel-Bienne, Switzerland. He is currently a Professor in control and signal processing with Bern University of Applied Sciences, Bern, Switzerland. His research interests

include various aspects of circuits and systems, statistical analysis, signal processing algorithms, and their hardware implementation, as well as the design of industrial control systems.



**Marcel Jacomet** received the M.Sc. and Dr. sc. techn. degrees in electronic engineering from the Swiss Federal Institute of Technology (ETH), Zurich, Switzerland, in 1983 and 1990, respectively.

Before joining Bern University of Applied Sciences (BFH) in 1992, he was responsible for the introduction of new technologies at Muller-Martini Electronics, Inc., Zofingen, Switzerland. He is currently a Professor in microelectronics with Bern University of Applied Sciences (BFH), Biel, Switzerland, and currently the Head of the BFH research institute Human Centered Engineering. His research interests include numerous projects in the fields of fuzzy logic, RFID, biometric recognition algorithms, chip design, and hardware algorithms with focus on medical applications. He and his team have been honored with the ETH/McKinsey prize as well as twice with the Swiss Technology Award.



**Hildegard Tanner** received the M.D. degree from the University of Bern, Bern, Switzerland, in 1994.

She is currently an Associate Professor in cardiology and the Deputy Head of clinical electrophysiology with the Department of Cardiology, the University Hospital, Inselspital, Bern, Switzerland. She is a Senior Lecturer with the Medical Faculty of the University of Bern, Bern, Switzerland. Her research interests include noninvasive and invasive diagnosis of cardiac arrhythmias and interventional treatment of cardiac arrhythmias.

Prof. Tanner is a member of the Swiss Working Group of Cardiac Pacing and Electrophysiology, the Swiss Society of Cardiology, the European Society of Cardiology, the European Heart Rhythm Association, the Heart Rhythm Society, and is the Vice-President of the Interest Group Women in Cardiology Switzerland.



**Andreas Haeblerlin** received the M.D. degree from the University of Bern, Bern, Switzerland, in 2009, and the Ph.D. degree in biomedical engineering and the Diploma of Advanced Studies in statistics, both in 2014.

He is currently the Head of the Group for Translational Electrophysiology, Bern University Hospital, Bern, Switzerland, and a fellow in invasive cardiac electrophysiology. He is a Lecturer in the Master's program "Biomedical Engineering" at the University of Bern. His research interests include translational

electrophysiology, in particular related to novel devices for the diagnosis and treatment of cardiac arrhythmias. He is a Member of the Swiss Society of Cardiology, the European Society of Cardiology, and the European Heart Rhythm Association.



**Hans-Andrea Loeliger** (S'85–M'92–SM'03–F'04) received the Diploma in electrical engineering and the Ph.D. degree in 1992 from ETH Zurich, Zurich, Switzerland. From 1992 to 1995, he was with Linköping University, Linköping, Sweden. From 1995 to 2000, he was a Full-Time Technical Consultant and Co-owner of a consulting company, from where he returned to ETH in 2000. He is a Professor with the Department of Information Technology and Electrical Engineering, ETH Zurich, Zurich, Switzerland. His research interests include the broad areas of

signal processing, machine learning, information theory, error correcting codes, communications, and electronic circuits.